MAJOR PAPER

Abnormal Flow Dynamics Result in Low Wall Shear Stress and High Oscillatory Shear Index in Abdominal Aortic Dilatation: Initial *in vivo* Assessment with 4D-flow MRI

Yasuo Takehara[1,*], Haruo Isoda[2], Mamoru Takahashi[3], Naoki Unno[4],
Norihiko Shiiya[5], Takasuke Ushio[6], Satoshi Goshima[6], Shinji Naganawa[7],
Marcus Alley[8], Tetsuya Wakayama[9], and Atsushi Nozaki[9]

Purpose: To characterize the non-laminar flow dynamics and resultant decreased wall shear stress (WSS) and high oscillatory shear index (OSI) of the infrarenal abdominal aortic dilatation, cardiac phase-resolved 3D phase-contrast MRI (4D-flow MRI) was performed.

Methods: The prospective single-arm study was approved by the Institutional Review Board and included 18 subjects (median 67.5 years) with the dilated infrarenal aorta (median diameter 35 mm). 4D-flow MRI was conducted on a 1.5T MRI system. On 3D streamline images, laminar and non-laminar (i.e., vortex or helical) flow patterns were visually assessed both for the dilated aorta and for the undilated upstream aorta. Cardiac phase-resolved flow velocities, WSS and OSI, were also measured for the dilated aorta and the upstream undilated aorta.

Results: Non-laminar flow represented by vortex or helical flow was more frequent and overt in the dilated aorta than in the undilated upstream aorta ($P < 0.0156$) with a very good interobserver agreement (weighted kappa: 0.82–1.0). The WSS was lower, and the OSI was higher on the dilated aortic wall compared with the proximal undilated segments. In mid-systole, mean spatially-averaged WSS was 0.20 ± 0.016 Pa for the dilated aorta vs. 0.68 ± 0.071 Pa for undilated upstream aorta ($P < 0.0001$), and OSI on the dilated aortic wall was 0.093 ± 0.010 vs. 0.041 ± 0.0089 ($P = 0.013$). The maximum values and the amplitudes of the WSS at the dilated aorta were inversely proportional to the ratio of dilated/undilated aortic diameter ($r = -0.694$, $P = 0.0014$).

Conclusion: 4D-flow can characterize abnormal non-laminar flow dynamics within the dilated aorta *in vivo*. The wall of the infrarenal aortic dilatation is continuously and increasingly affected by atherogenic stimuli due to the flow disturbances represented by vortex or helical flow, which is reflected by lower WSS and higher OSI.

Keywords: *4D-flow, phase-contrast image, abdominal aortic aneurysm, wall shear stress, oscillatory shear index*

[1]Department of Fundamental Development for Advanced Low Invasive Diagnostic Imaging, Nagoya University Graduate School of Medicine, Aichi, Japan
[2]Department of Brain & Mind Sciences, Nagoya University Graduate School of Medicine, Aichi, Japan
[3]Department of Radiology, Seirei Mikatahara General Hospital, Shizuoka, Japan
[4]Department of Vascular Surgery, Hamamatsu Medical Center, Shizuoka, Japan
[5]First Department of Surgery, Hamamatsu University School of Medicine, Shizuoka, Japan
[6]Department of Diagnostic Radiology & Nuclear Medicine, Hamamatsu University School of Medicine, Shizuoka, Japan
[7]Department of Radiology, Nagoya University Graduate School of Medicine, Aichi, Japan
[8]Department of Radiology, Stanford University School of Medicine, CA, USA
[9]MR Applications and Workflow, GE Healthcare Japan, Tokyo, Japan

*Corresponding author: Department of Fundamental Development for Advanced Low Invasive Diagnostic Imaging, Nagoya University, Graduate School of Medicine, 65, Tsurumai-cho, Showa-ku, Nagoya, Aichi 466-8550, Japan. E-mail: takehara@med.nagoya-u.ac.jp

Introduction

Aortic aneurysms were the primary cause of 9863 deaths in 2014[1] and a contributing cause in more than 17,215 deaths in the United States in 2009 (https://wonder.cdc.gov/ucd-icd10.html). Although there are many sorts of abdominal aortic aneurysm (AAA) in their etiologies, atherosclerosis is the primary pathogenesis creating AAA.[2–4]

Concerning the risk of rupture of an AAA, aneurysmal size is closely linked, i.e., size >5 cm in diameter is around 20%, >6 cm approximately 40% and >7 cm over 50%.[5] Therefore, surgical repair or endovascular repair (EVAR) is recommended for an AAA more than 5 cm in diameter.[6]

Previous studies have shown that laminar flow with consistent and relatively high velocity is required to maintain the integrities of the arterial wall,[7–13] where the arterial endothelial cells play an essential role as a mechanoreceptors[14–21] of flow velocity by detecting wall shear stress (WSS).[22–26] A certain level of WSS is necessary for stimulating atheroprotective

pathways by controlling various chemical mediators.[14–21,27] A high oscillatory shear index (OSI) that reflects fluctuations in WSS induces an inflammatory response, including an increase in reactive oxygen species.[28,29] Atherosclerosis results in vascular diseases, including penetrating atherosclerotic ulcers, arteriosclerosis obliterans, or aortic aneurysm.

Abdominal aortic aneurysm is characterized by an abrupt dilatation of the flow path of the abdominal aorta, which breaks critical Reynolds number and resultant non-laminar flow. Previously, WSS and OSI of the AAA had been assessed by personalized morphology using magnetic resonance angiography (MRA) and boundary conditions with the use of cardiac phase-resolved 2D phase-contrast MRI (2D PC cine MRI), which were performed exclusively with the aid of simulated calculation of computational fluid dynamics (CFD).[30] The recently innovated cardiac phase-resolved three-dimensional (3D) phase-contrast MRI (4D-flow MRI) is a 3D phase-contrast imaging that can provide comprehensive 3D velocity information of the blood flow within the entire vasculatures throughout the cardiac cycle.[31–34] Unlike CFD simulation, the 4D-flow MRI allows for direct measurements of the WSS and OSI by transforming actual local 3D velocity data measured adjacent to the endothelium.[35–37]

With an aid of 4D-flow MRI, the purpose of this study was to characterize non-laminar flow dynamics represented by vortex or helical flow, as well as their derivatives such as WSS and OSI in the dilated abdominal aorta as compared with the upstream undilated aorta.

Materials and Methods

The prospective single-arm study using no surgical or pharmacological interventions was approved by the Institutional Review Board (IRB). The study recruited 23 consecutive patients with infrarenal abdominal aortic dilatation diagnosed by contrast-enhanced CT performed from July 1, 2008, to June 30, 2009. Abdominal aortic dilatation was simply defined as the diameter of the aortic portion is larger than that of the upstream abdominal aorta. Five patients dropped out of the study for the following reasons. Two patients declined contrast administration, 1 had a pacemaker placement, one had an urgent surgical stent placement before MRI, and there was lost flow data storage in one due to the hard disk break down of the computer.

Consequently 18 patients remained at the endpoint of the study. All the patients provided written informed consent. The study population included 16 males and 2 females with age ranging from 52 to 85 years (median 67.5 years). There were one saccular and 17 fusiform aortic dilatation with maximum transverse diameters ranging from 25 to 43 mm (median 35 mm) and a maximum length ranging from 41 to 94 mm (median 67 mm). One patient fell short of the definition of "aneurysm" proposed by the Society for Vascular Surgery and the North American Chapter, International Society for Cardiovascular Surgery for aortic aneurysm and Japanese Circulation Society, which is maximum diameter ratio between the dilated aorta and the upstream undilated aorta is over 1.5.[38] Therefore, in this study, we deal with our study population as a whole "dilated abdominal aorta" instead of "AAA". For the individual case, the lesion is called AAA if the lesion matches the definition stated above.

All MRIs were conducted on 1.5T MR scanner (Signa infinity twin speed with Excite ver. XI; GE Healthcare, Waukesha, WI, USA) with an 8-channel body phased-array coil (GE Healthcare).

Time-resolved contrast-enhanced 3D MR angiography

Prior to 4D-flow MRI, contrast-enhanced 3D magnetic resonance angiography (MRA) was obtained after bolus injection of gadolinium chelate (Magnevist; Bayer Yakuhin, Osaka, Japan or Omniscan; Daiichi-Sankyo, Tokyo, Japan) with 0.1 mmol/kg with an injection rate of 2–3 mL/s using an autoinjector. The contrast administration was used for segmenting accurate arterial wall boundary for post-processing and additionally to increase the signal-to-noise ratio (SNR) in 4D-flow measurement. 3D fast spoiled gradient echo (3D-FSPGR)-based sequence was used with the following parameters: TR (ms)/TE (ms)/FA (°)/number of excitations (NEX) = 2.6/0.8/15/1, a field of view (FOV) of 48 cm × 33.6 cm, partition thickness of 2 mm with zero fill interpolation of 2, overlaps of 2 mm, a matrix of 224 × 224, receiver bandwidth (RBW) of 83.3 kHz, array spatial sensitivity encoding technique reduction factor of 2, 60 partitions × 6, and scan time of 35 s. The best arterial phase 3D data set with whole abdominal aortic opacification was picked out from the six phases and was used for the segmentation and the proper morphometry of the aortic wall.

Cardiac phase-resolved 2D phase-contrast MRI

Following contrast-enhanced 3D MRA, an electrocardiogram (ECG) gated, respiratory compensated, axial 2D PC cine MRI was also performed to validate the velocity data of 4D-flow MRI and to optimize velocity encoding (VENC) for 4D-flow. The cross-section was placed in the abdominal aorta above the renal artery using the following parameters: TR (ms)/TE (ms)/FA (°)/NEX of 29/auto (5)/30/2, RBW of 32 kHz, FOV (cm) of 16 × 16, a thickness of 4 mm, a matrix of 160 × 160, R–R phases of 30, VENC of 150 cm/s encoded in all directions.

Since the cardiac phase resolution for the 2D PC cine MRI was 30, it was adapted to 12 phases when compared with 4D-flow MRI.

Cardiac phase-resolved 3D phase-contrast MRI

Following 2D PC cine MRI, ECG gated, respiratory compensated cardiac phase-resolved 3D-FSPGR-based 4D-flow MRI was conducted covering the whole abdominal

aorta with the following parameters: TR (ms)/TE (ms)/FA (°)/NEX of 4.5–5.0/1.6–2.0/15/1, FOV (cm) of 34–48 × 34–48, a matrix of 224–256 × 160–224, partition thickness of 2 mm, 32–40 partitions, 12 phases, approximate imaging time of 10 min with a reduction factor of 2 for an autocalibrating reconstruction for Cartesian sampling.[39] The VENC was determined based on the maximum flow velocity value measured with 2D PC cine MRI added with +10 cm/s for a safety margin.

We used a 4D-flow MRI application developed at Stanford University as a research version and was operated following the restriction of the Japanese Ministry of Health, Labor and Welfare after IRB approval.

Post-processing of 4D-flow MRI data

4D-flow MRI data sets and 3D MRA data set were transferred to a personal computer (Intel Core i7 CPU, 3.2 GHz, 12 GB RAM, Microsoft Windows 7) in DICOM format, and were post-processed with flow analysis software (Flova; R'Tech, Shizuoka, Japan). The application was composed of two processes of segmentation and analysis. Velocity data were segmented using the boundary of the abdominal aorta depicted on 3D MRA. First, cardiac phase-resolved images of 3D velocity vector fields were generated to overview the blood flow within the abdominal aorta. Then, 3D streamlines, WSS maps, and OSI map were generated using 4D data sets.

Generating 3D streamlines

We chose several cross-sectional planes every 3 cm traversing the abdominal aorta perpendicular to the longitudinal axis of the aorta, including the dilated aorta and the upstream undilated aorta. We generated 3D streamlines using Runge–Kutta method.[40] 3D streamlines are integrated traces along the instantaneous velocity vector field, color-coded according to the local velocity magnitude.

Calculation of WSS and OSI

Wall shear stress is defined as the product of fluid viscosity and shearing velocity of the adjacent vascular wall. Our method to calculate the shearing velocity vector is similar to those reported by Cheng et al.[41] or Masaryk et al.[42]; however, our method is not two dimensional but three dimensional. The 3D method to measure WSS has previously been reported by Isoda et al.[43] Our application is based on the same platform as Isoda's method. The dynamic viscosity of the blood was assumed to be 0.00384 Pa in the application.

Oscillatory shear index that reflects instantaneous fluctuation of WSS was calculated by temporal changes of the local WSS vector. OSI is defined as $(1 - |\int \mathbf{wss}_i dt| / [\int |\mathbf{wss}_i| dt])/2$, where $\mathbf{wss}_i$ is instantaneous WSS vectors.[44] OSI ranges from 0 to 1/2, and a large OSI means that instantaneous WSS vectors are much fluctuated compared with that of the mainstream direction at the calculated point during one cardiac cycle.

Measurement of the geometrical features of the abdominal aorta

The maximum luminal diameter and the length of the dilated aorta were measured on the workstation using multiplanar reformatted images with the exclusion of the thickness of the mural thrombus. Likewise, the maximum luminal diameter of the upstream undilated abdominal aorta was also measured, selecting a similar level as 2D PC cine was measured. The measurements were performed by 2 experienced radiologists (Y.T. and M.T.) in consensus on the reformatted image using the arterial phase 3D MRA data set, and then the values were averaged. Then the diameter ratio (maximum diameter of the dilated aorta)/(maximum diameter of the undilated upstream abdominal aorta) was calculated. Experienced radiologists (Y.T. and R.H.) measured the immediate upper bent angle formed by the middle lines of the undilated and the dilated aorta in consensus (Fig. 1).
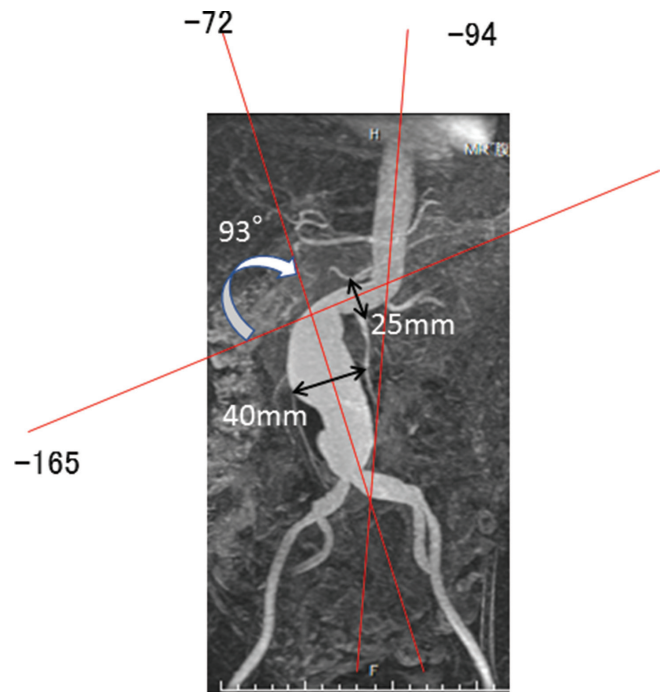
Fig. 1 The scheme of the measurements of the values reflecting geometrical features of the abdominal aortic aneurysm. The example of auxiliary lines delineated on the enhanced 3D MRA of a 68-year-old female. The maximum luminal diameter (40 mm) and the length of the dilated segment as well as the diameter of upstream non-dilated aorta (25 mm) were measured. The immediate upper bent angle created by the middle lines of the dilated segment and the undilated segment (93°) was also measured. MRA, magnetic resonance angiography.

Measurements of the flow velocities

The cross-sectional region of interest (ROI) was created in the dilated aorta as well as in the upstream undilated portion of the aorta, and the cardiac phase-resolved spatially-averaged flow velocities perpendicular to the sections were measured with 4D-flow MRI. The measurements in the upstream undilated aorta were performed at similar cross-sectional ROIs prescribed for 4D-flow MRI. The mean time-resolved velocities were also measured with 2D PC cine MRI for reference. The ROIs were placed so that the planes were perpendicular to the middle lines of each aortic segment.

Evaluation of the flow patterns

Two radiologists (Y.T. and M.T.) visually assessed the flow patterns seen in the dilated aorta and the upstream undilated segment of the abdominal aorta by viewing the streamlines in terms of the presence or absence and the degree of non-laminar flow specifically concerning vortex and helical flow separately at systole and diastole. The assessments were performed independently and in a blinded fashion. The degree of abnormal flow patterns were rated as follows: (1) none to mild; consistent laminar flow or non-laminar flow with maximum diameters less than one-third of the aortic diameter (Fig. 2a), (2) moderate; one abnormal flow patterns involving more than one-third of the aortic lumen (Fig. 2b) and (3) severe; more than two non-laminar flow patterns involving more than one-third of the aortic lumen (Fig. 2c). The rating was performed separately for systole and diastole. The abnormal flow patterns could be instantaneous or prolonged during the period of observations. 3D streamline images, including all cardiac phases were available on the monitor display of a workstation enabling the observation of the largest diameter of the flow patterns.
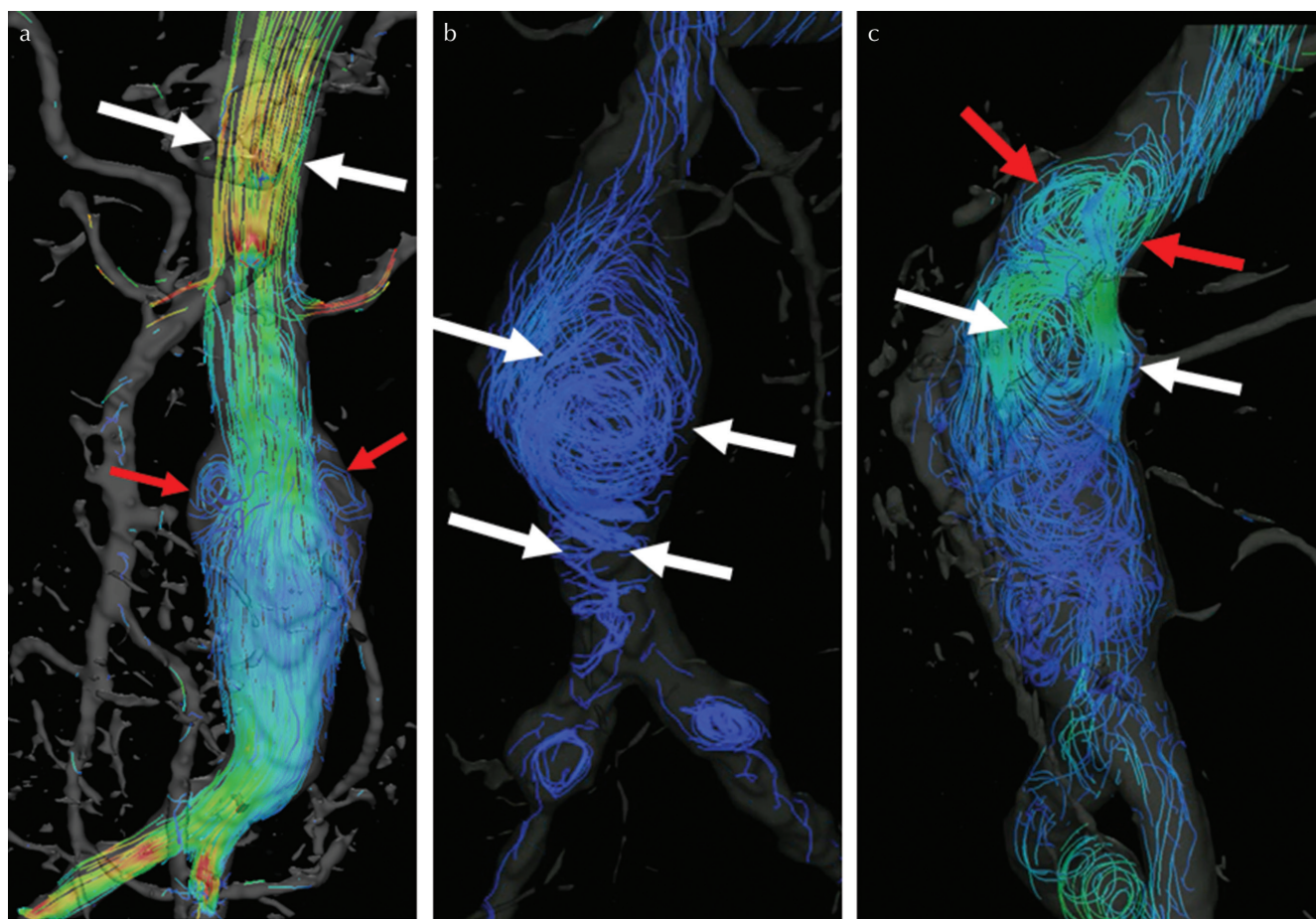
Fig. 2 (**a**)–(**c**) The examples of the ratings for laminar or non-laminar flow observed on streamline analysis. (**a**) Streamline analysis for the AAA of a 84-year-old male at systole. Laminar flow at the upstream undilated aorta (white arrows) and the tiny vortices (red arrows) with diameter less than one-third of the aneurysmal diameter at the shoulder of the AAA are seen. The degree of non-laminar flow were both rated as none to mild. (**b**) Streamline analysis for the AAA of a 68-year-old male at diastole. A large helical flow (white arrows) occupying more than one-third of the AAA diameter was rated moderate (Although the helical flow was over one-third of the aneurysm, it was single). (**c**) Streamline analysis for the AAA of a 60-year-old male at diastole. There are more than two large vortices (white arrows and red arrows) with size over one-third of the aneurysmal diameter at the proximal portion of the AAA, which were rated as severe non-laminar flow. Supplementary movie shows hemodynamics over one cardiac cycle using streamline analysis. AAA, abdominal aortic aneurysm.

Measurements of the WSS and the OSI of the aortic wall

Wall shear stress and oscillatory shear index were measured on the cardiac phase-resolved 3D WSS distribution maps and 3D OSI distribution map, placing a circumferential area ROI covering the whole dilated portions of the abdominal aorta and the undilated upstream portions of the abdominal aorta separately (Fig. 3). For the ROI of the upstream undilated segment, a level was selected, giving the maximum surface area avoiding the stump of the aorta, as high up as possible, but under the level of the diaphragm. We compared the differences in cardiac phase-resolved spatially-averaged WSS of each cardiac phase as well as OSI of each dilated aorta and their upstream undilated segments.
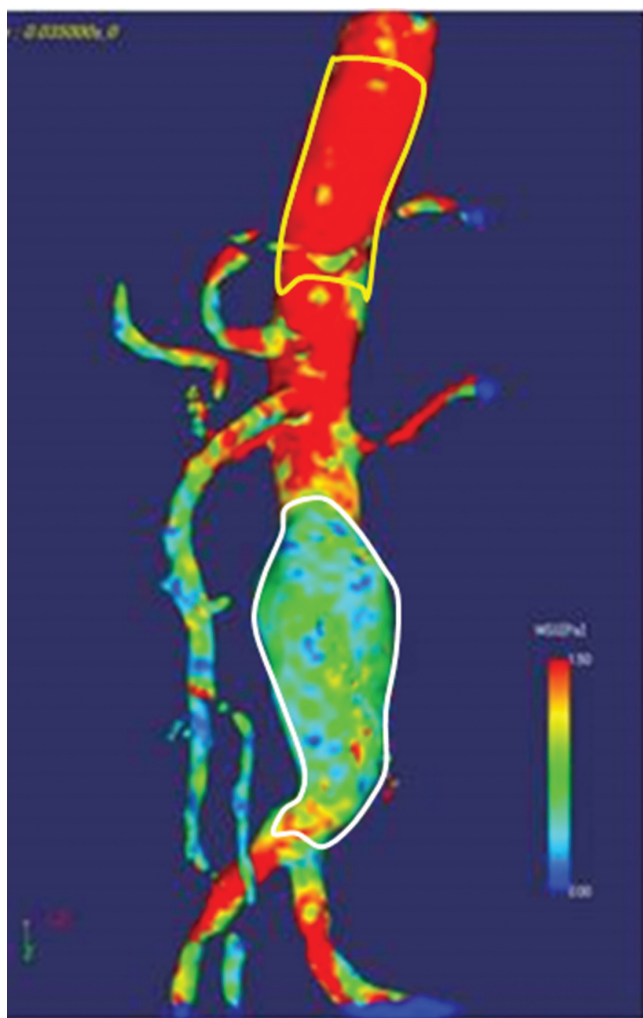
Fig. 3 A color coded 3D WSS map of a 84-year-old male AAA patient shows the range of abdominal aorta imaged on 4D-flow MRI. WSS was measured on the 3D map covering circumferential area of the dilated (surrounded by white line) vs. non-dilated upstream aorta (surrounded by yellow line). Note: dilated portion (WSS coded blue to green) is considerably lower WSS than the non-dilated segment (higher WSS coded red). AAA, abdominal aortic aneurysm; WSS, wall shear stress.

Statistics

All numerical data were expressed as mean ± standard error (SE) when normally distributed or otherwise expressed as median ± SE. The mean velocities and the WSS measurements for each cardiac phase were evaluated with a repeated-measure analysis of variance (ANOVA) followed by the Dunnett's test. Differences in the mean velocities and the spatially averaged WSS and OSI of the dilated aorta and the undilated upstream aorta were analyzed using a Student's paired t-test, where Bartlett's test indicated homogeneity of variance, or otherwise by non-parametric Wilcoxon test. The rated abnormal flow patterns between the dilated aorta and the undilated upstream abdominal aorta were assessed with a non-parametric Wilcoxon test combining the assessments by two observers. The regression analysis for correlation of the dilated aortic diameter ratio and mid-systolic WSSs or amplitude of WSSs (i.e., maximal WSS minus minimal WSS) was assessed with Spearman's test. A P-value <0.05 was taken as statistically significant. Inter-observer variability was assessed with weighted kappa statistics. Kappa values below 0.2 were interpreted as poor, 0.21–0.40 fair, 0.41–0.60 moderate, 0.61–0.8 good, and 0.81–1.00 were interpreted as very good agreement. Statistical analyses were performed with the use of StatFlex (Artech, Osaka, Japan) or Medcalc (Medcalc software, Ostend, Belgium).

Results

The geometrical features of the abdominal aorta were as follows: the median length (mm): 64 ± 3.5; maximum diameters of the dilated aorta (mm): 34 ± 1.1; the maximum diameter of the upper undilated aorta (mm): 21 ± 0.51; diameter ratio: 1.7 ± 0.063 and immediate upper bent angle (°): 25 ± 7.1.

The cardiac phase-resolved spatially-averaged flow velocities at the levels of the dilated aorta and the upstream undilated aorta measured with 4D-flow MRI and cardiac phase-resolved 2D PC cine MRI are shown in Fig. 4. The agreement of the mean velocities measured with the two methods was reasonably good (<8.6% difference) at mid-systole, and there was almost perfect agreement during diastole. The values (mm/s) within the undilated upstream aorta, systolic initial six phases (70 ± 8.5, 105 ± 12, 174 ± 17, 191 ± 17, 145 ± 14, 81 ± 10) were significantly higher than end-diastole (10th phase 43 ± 7.8; $P < 0.0001$). Similarly, within the dilated aorta, the values at systolic five phases were significantly higher than that of end-diastole (41 ± 6.6, 62 ± 7.7, 71 ± 8.3, 55 ± 6.6, 32 ± 5.6; $P < 0.0001$) (Fig. 4). The flow velocities in the dilated aorta were significantly lower than upstream undilated abdominal aorta at all cardiac phases.

The flow patterns in the dilated aorta versus in the undilated aorta were distinctly different. Inside the dilated aorta, the appearances of non-laminar flow patterns such as vortex ($P = 0.0156$) were more prominent during systole, and vortex ($P = 0.0001$) and helical flow ($P = 0.0074$) during diastole (Fig. 5a and 5b). Typically, during systole, non-laminar flow dominates

Mean Velocities in the Aorta Measured with 4D-Flow and 2D-PC cine
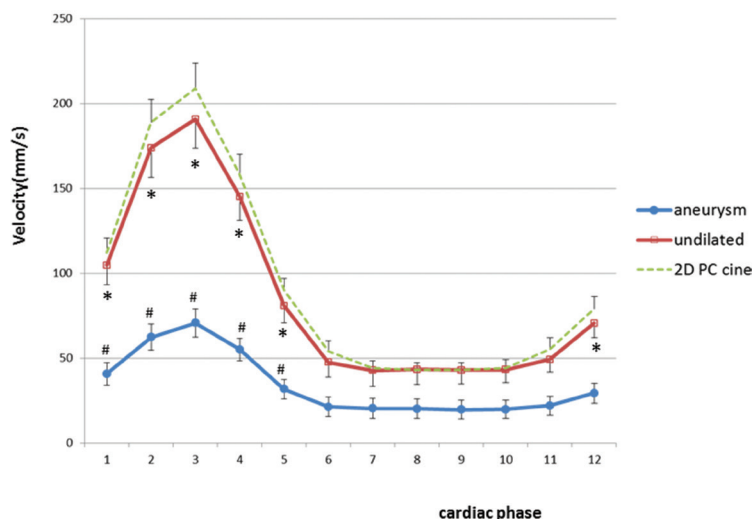
Fig. 4 Graph shows time-resolved mean velocity values perpendicular to the cross sections of the ROI in the aneurysm (closed circle) and upstream undilated aortic segment (open square) measured with 4D-flow MRI. The velocity in the upstream undilated aorta measured with time-resolved 2D PC cine MRI dotted line is also shown for reference. The agreements of the velocities measured using 4D-flow and the 2D PC cine MRI were reasonably good, being identical in the diastole and up to 8.6% difference in the mid-systole. The values within the undilated upstream aorta, systolic six phases (*) were significantly higher compared with end-diastole (10th phase). Similarly, the values within the aneurysm at the systolic five phases (#) were significantly higher than those of end-diastole. The mean velocities in the aneurysm are significantly lower than those in the undilated upstream aorta throughout the entire cardiac cycle. Bars are shown in SE. The original phase resolution for the 2D PC cine MRI (30 phases/s) was adapted to 12 phases to compare with that of 4D-flow MRI. 2D PC cine MRI, 2D phase contrast MRI; 4D-flow MRI, 3D phase-contrast MRI; ROI, region of interest; SE, standard error.

dilated aorta; however, the laminar flow patterns were maintained, and none of the vortex or helical flow appeared within the upstream undilated portions (Figs. 2, 5a, 5b, 6 and 7). There was very good agreement between the two observers concerning the ratings of the laminar or non-laminar flow dynamics such as vortex or helical flow during systole and diastole for dilated aorta and undilated upstream aorta (weighted kappa values ranging from 0.824 to 1) (Fig. 5a and 5b).

Concerning the temporal changes of the mean spatially-averaged WSS measured in the dilated aorta and the undilated upstream aorta, the values during systolic seven phases were significantly higher than that of end-diastole ($P < 0.001$) (Fig. 8).

The spatially-averaged WSS of the dilated aorta was significantly lower ($P < 0.001$) than that of the undilated upstream aorta in all cardiac phases. In mid-systole (third phase), mean spatially-averaged WSS was 0.20 ± 0.016 Pa for the dilated aorta vs. 0.68 ± 0.071 Pa for undilated upstream aorta ($P < 0.0001$), and in the end-diastole (10th phase) it was 0.10 ± 0.008 Pa for aneurysm vs. 0.18 ± 0.018 Pa for undilated upstream aorta ($P = 0.0003$) (Fig. 8).

There was a moderately good inverse correlation between the dilated aortic diameter ratio and the maximal WSS (mid-systole) of the dilated aorta [$r = -0.542$, $P = 0.0203$, confidence interval (CI): -0.805, -0.010] (Fig. 9a). The amplitude of WSS showed even better inverse correlation with the dilated aortic diameter ratio of the AAA ($r = -0.694$, $P = 0.0014$, CI: -0.877, -0.335) (Fig. 9b).

Oscillatory shear index which reflects the fluctuation of the WSS during the cardiac cycle was greater in the dilated aorta (0.093 ± 0.010, CI: 0.08, 0.11) as opposed to the upstream undilated aorta (0.041 ± 0.0089, CI: 0.012, 0.059; $P = 0.013$) (Fig. 10).

The immediate upper bent angle (median $24.5° \pm 7.1°$) did not affect geometrically averaged WSS or OSI of the dilated aorta with statistical significance; however, in some selected cases, it was considered to have been affecting local WSS or OSI (Fig. 6a–6c).
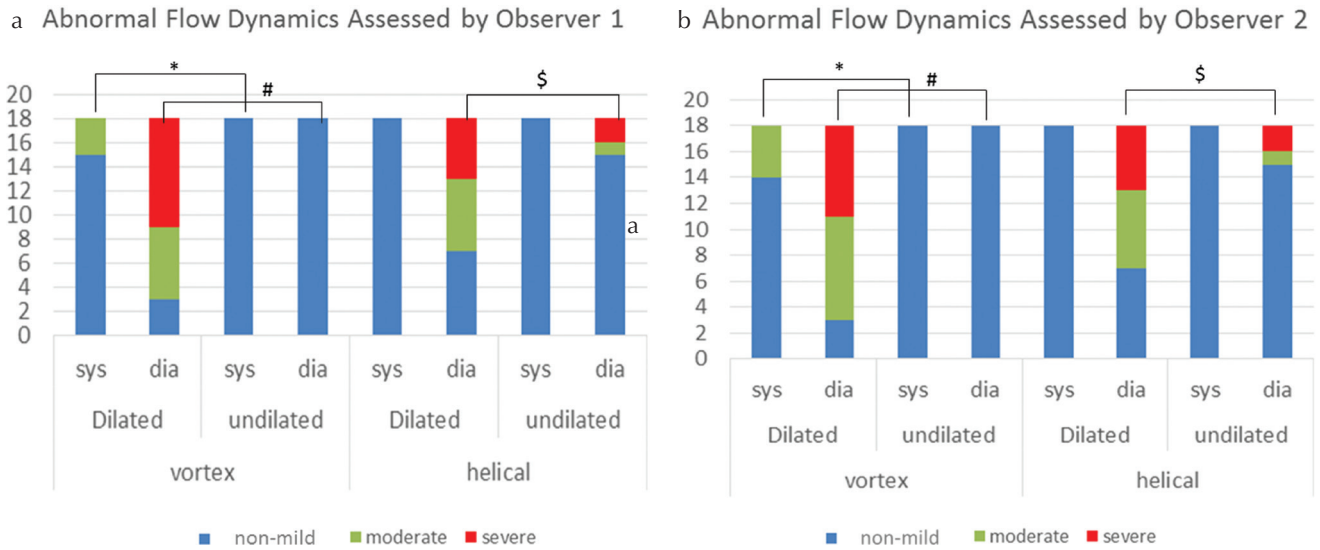
Discussion

Although many proven biochemical factors promote atherogenesis, hemodynamic stress on the aortic wall has also been considered as a key contributor. Generally, both atherosclerosis and aneurysm have a preference for developing in specific locations within the vascular tree, such as branch points and areas of curvature where flow disturbance occurs.[45–47] In such locations, the laminar flow becomes non-laminar, where low WSS and high OSI affects vascular wall with atherosclerosis.[48–50]

In humans, atherosclerotic lesions are more prevalent in the infrarenal aorta than the suprarenal aorta.[45] Approximately 90% of all AAAs are associated with atherosclerosis, and 95% of AAAs develops in the infrarenal aorta. Infrarenal AAA comprises more than 80% of all aortic aneurysms.[51] The reasons for these regional preferences in susceptibility have been unknown and remain a challenge in research.[52,53]

Our study verified that the flow patterns in undilated segments of the abdominal aorta are characterized by fast, consistent laminar flow and its mean WSS of 0.68 Pa during the mid-systole (temporal average of 0.44 Pa) is within the range of previously reported values (0.34–1.04 Pa) measured in the suprarenal aorta.[54,55] It is also notable that the laminar flow is dominant, and non-laminar flow occurs only during the brief period of diastole in the undilated upstream segment. On the contrary, the flow patterns in the dilated aorta are characterized by non-laminar flow such as vortex or helical even during the systole. In the literature, the low WSS and high OSI due to the non-laminar flow have been suggested by CFD simulation.[56] The stagnant flow within AAA is recently reported by Ziegler et al.[57] They used 4D-flow to measure the blood flow velocity reflected by the time travel distances of the blood

a Abnormal Flow Dynamics Assessed by Observer 1

b Abnormal Flow Dynamics Assessed by Observer 2

non-mild moderate severe

Fig. 5 (**a**) and (**b**) The appearances and the severity of the abnormal flow patterns observed within the aneurysm and the undilated upstream segment of the abdominal aorta. (**a**) Three grades of non-laminar flow dynamics (none to mild, moderate and severe) were rated by observer 1. (**b**) The same assessments rated by observer 2. *, #, $: significantly higher rates than undilated upstream segments (*: P = 0.0156 #: P = 0.0001, $: P = 0.0074). The comparisons were made using integrated data of observer 1 and 2. dia, diastole; sys, systole.
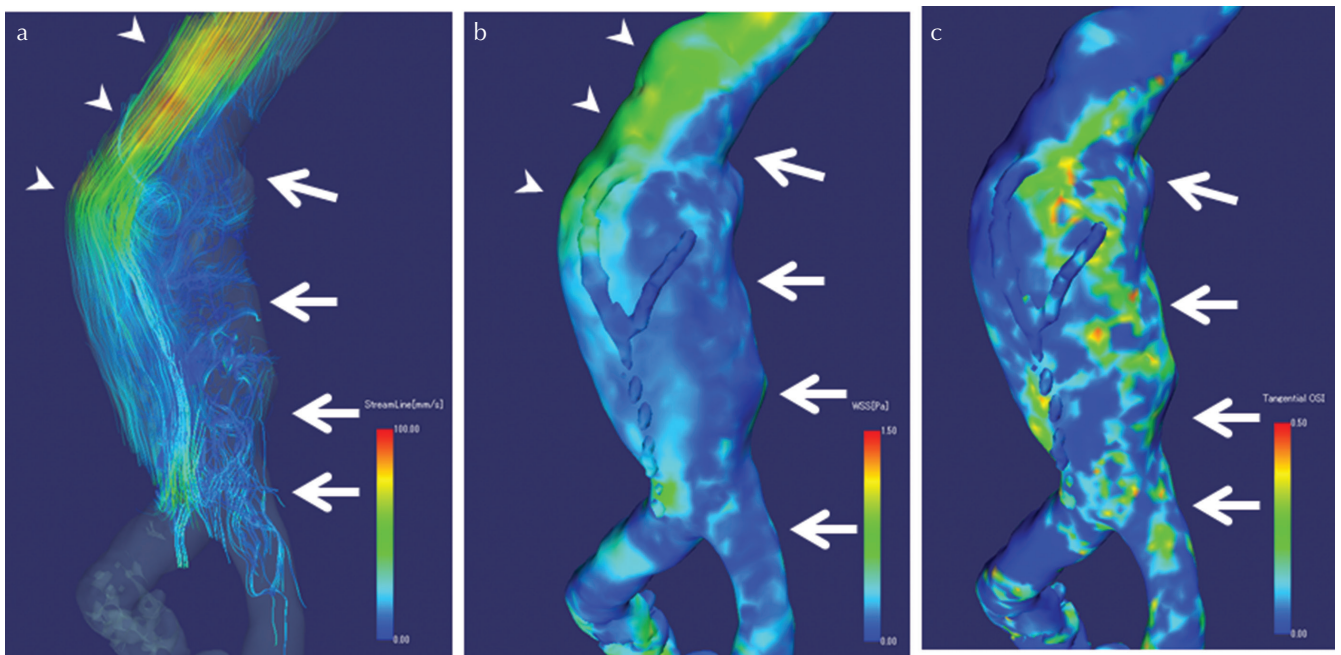
Fig. 6 (**a**)–(**c**) Color-coded 3D reconstruction images at systole of a 60-year-old male with AAA shown as a left anterior oblique projection. Flow analysis software was used to produce these 3D interposed images on 3D MRA model. There is a bending (bent angle of 38°) and an abrupt diameter increase (diameter ratio 1.7) in the lumen of the abdominal aorta. Note: upper bent angle created non-laminar flow in the left half of the aorta and consequent decreased WSS and the increased OSI of the corresponding aortic wall (arrows). (**a**) The streamline image shows fast laminar flow within the undilated upstream segment (arrowheads); however, the velocities decrease once the flow enters the aneurysm. The bending and dilatation of the flow area affect the integrity of the flow patterns. The lost momentum of the flow causes vortex flow (arrows), where it coincides with low WSS (**b**). (**b**) A WSS map shows the aneurysmal wall particularly on the inner curvature of the aneurysm, which is coded blue, has a lower WSS (arrows) than the upstream undilated segment, which is coded green (arrowheads). (**c**) An OSI map of the same case shows a high OSI (coded red to green) where vortex flow were observed in the vicinity. Note left half of the aneurysm (arrows) shows higher OSI. AAA, abdominal aortic aneurysm; MRA, magnetic resonance angiography; OSI, oscillatory shear index; WSS, wall shear stress.
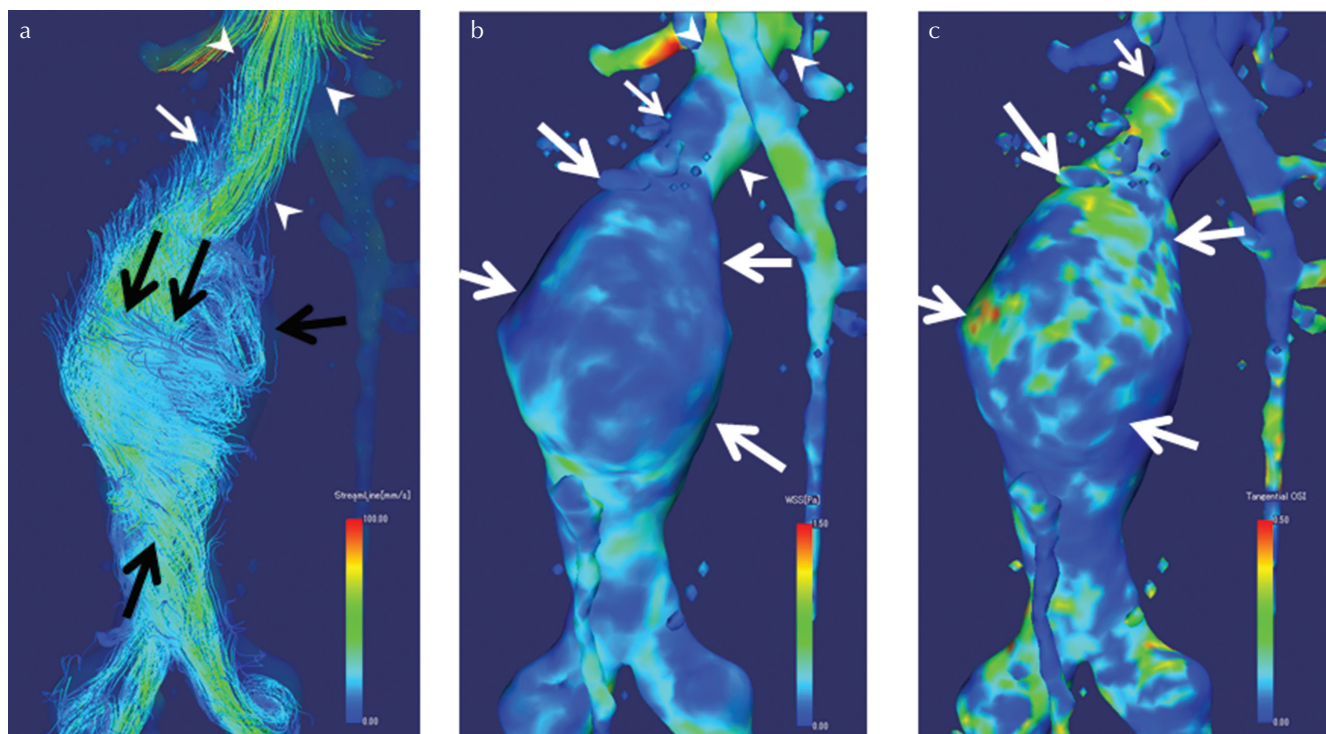
Fig. 7 (**a**)–(**c**) Anterior projection of the color coded 3D image of a 68-year-old male with AAA at mid-systole. There is a subtle bending and abrupt diameter increase in the lumen of the abdominal aorta. In this particular case, there is a large helical flow flowing across the entire aortic width; therefore resulted in relatively homogenous reduction of the WSS and increased OSI. (**a**) The streamline image shows laminar flow within the undilated upstream segment (arrowheads); however, large helicities (arrows) dominates the entire aneurysmal cavity and partially of its neck (small arrow). Again, the bent and the dilatation of the flow area seem to be affecting the integrity of the flow pattern. (**b**) A WSS map shows diffuse low WSS of the aneurysmal wall (arrows) and a part of its neck (small arrow) which are coded blue as compared with the upstream undilated segment coded green (arrowheads). (**c**) An OSI map shows a high OSI (arrows; coded red to green) in the aneurysm and a part of its neck (small arrow) corresponding to the low WSS patterns and abnormal flow patterns. AAA, abdominal aortic aneurysm; OSI, oscillatory shear index; WSS, wall shear stress.
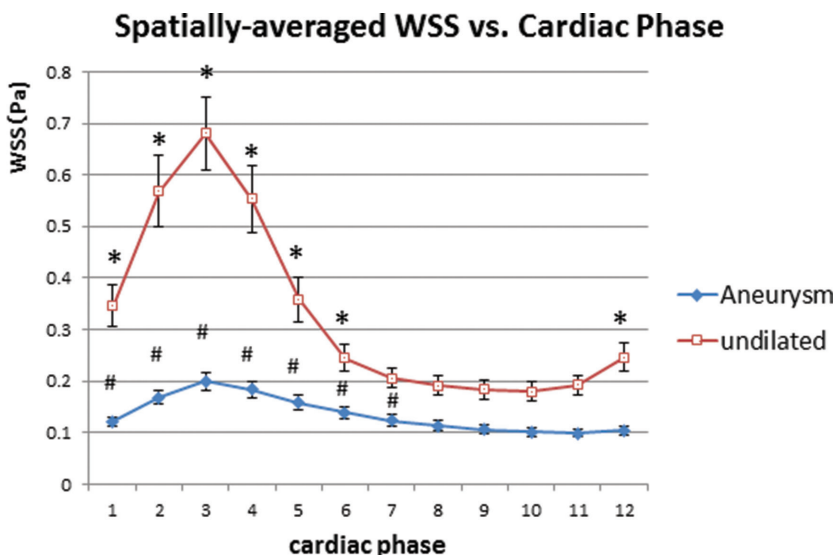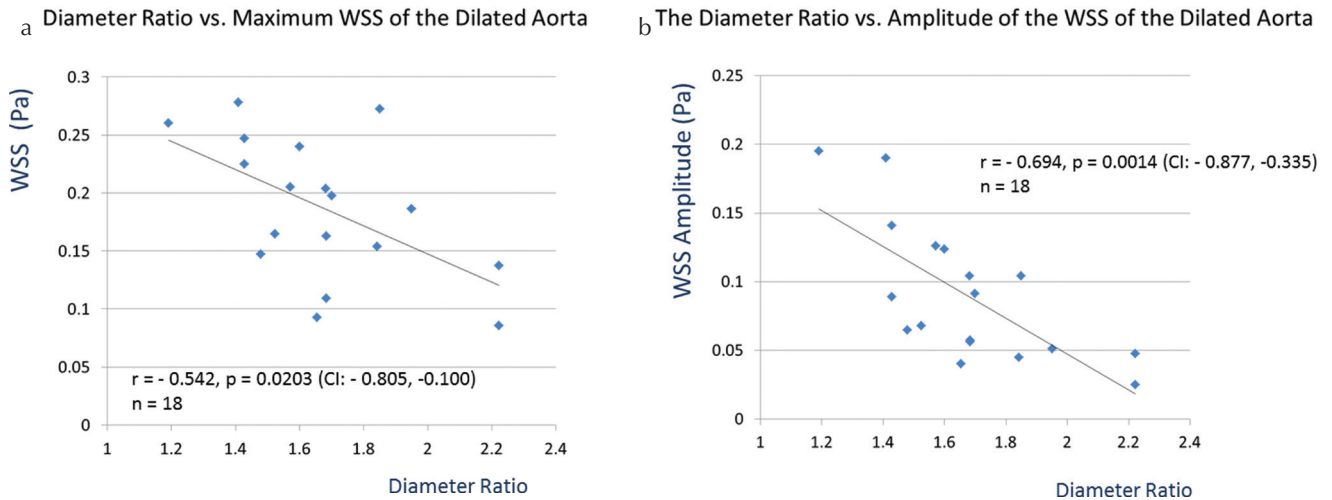

Fig. 8 The time (cardiac phase) course changes of spatially-averaged WSS through a cardiac cycle measured in the aneurysm and the undilated upstream aorta. The mean spatially-averaged WSSs of the undilated upstream aorta were significantly higher during systolic seven phases (*) than the end-diastole (10th phase). The spatially-averaged WSSs of the aneurysm during systolic seven phases (#) were significantly higher than end-diastole. The spatially-averaged WSSs in the aneurysms were significantly lower ($P < 0.001$) than those of the undilated aortic segments of the proximal aorta in all cardiac phases (not marked on the graph). WSS, wall shear stress.

flow *in vivo*. We also found that non-laminar flow is dominant, and WSS of this portion is lower and OSI higher than those of the upstream undilated segments. The flow dynamics in the AAA can be well explained by a typical fluid dynamics theory with the model of "a pipe of sudden enlargement".[58,59] In fluid mechanics theory, flow separation will decrease the

a **Diameter Ratio vs. Maximum WSS of the Dilated Aorta**

b **The Diameter Ratio vs. Amplitude of the WSS of the Dilated Aorta**

Fig. 9 (**a**) and (**b**) The relationship between dilated/undilated aorta diameter ratio vs. WSS. (**a**) The maximum WSS (at mid-systole) showed moderately good correlation to the diameter ratio [$r = -0.542$, $P = 0.0203$, confidence interval (CI): -0.805, -0.010). (**b**) The amplitude of WSS, i.e., minimum WSS subtracted from maximum WSS showed a better inverse correlation to the diameter ratio ($r = -0.694$, $P = 0.0014$, CI: -0.877, -0.335). WSS, wall shear stress.
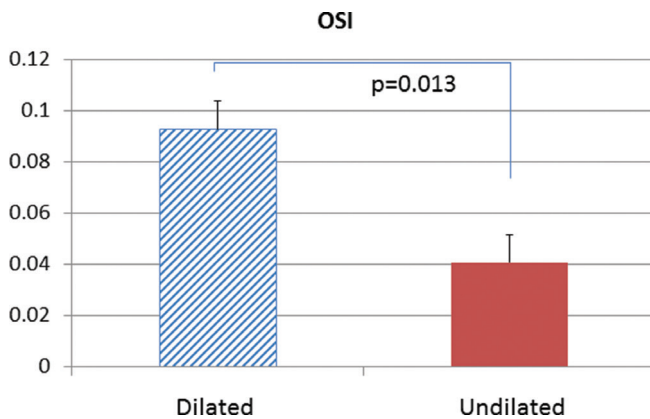
Fig. 10 OSI which reflects the fluctuation of the WSS during the cardiac cycle was higher in the dilated aorta (0.093 ± 0.010, CI: 0.080, 0.11) compared with the proximal undilated portion (0.041 ± 0.0089, CI: 0.012, 0.059; $P = 0.013$). OSI, oscillatory shear index; WSS, wall shear stress.

momentum of the flow in the abruptly enlarged space. The stagnant fluid mass that lost momentum in the dilated pipe is pushed back by the backflow of the stream from the downstream fluid mass, which creates turbulent eddies at the shoulder and the marginal portions of the lumen adjacent to the wall of the dilated pipe.[60–62] The loss of momentum is proportional to the increase in the cross-sectional area of the pipe, which is known as Borda–Carnot theory.[61] This phenomenon was well documented also in this *in vivo* study (Figs. 6a–6c, 7a–7c, 9a and 9b). While the blood is flowing within the undilated aorta, in mid-systole, the blood flow can maintain consistent laminar flow; however, once the flow enters into a larger flow path of the aneurysm, the non-laminar flow represented by vortex or helical flow occurs. In our study, WSS is inversely proportional to the diameter ratio (Fig. 9a and 9b),

which was well explained by the fluid dynamics theory stated above. The tortuosity or bent of the aorta is another challenge to the integrity of the blood flow. At the edge of the separated boundary layer, where the velocities change direction, a line of vortices occurs, which is known as a vortex sheet. This boundary layer flow separation and increase in the stagnant flow due to the vortices results in substantial energy losses in the flow. These separating divergent flows are inherently unstable, and far more energy is lost than in parallel or convergent flow.[59] As AAA grows, the junction of the dilated and undilated segment is elevated or shifted right or left, which creates the bent of the flow area even more.

The results of the current study suggest that a dilated infrarenal aorta hinders the maintenance of laminar flow, and is responsible for non-laminar flow such as vortex or helical, which results in lower WSS and higher OSI. If the hemodynamic abnormality leads to the propagation of atherogenic processes in the aorta that weaken the dilated aortic wall, it may result in progressive dilatation of the aneurysm, and this may again accelerate the non-laminar flow. This interaction causes a vicious cycle that can consequently cause aneurysmal growth and eventual rupture.

It is difficult to specify what the initiating stimulus for aortic dilatation is. However, from the hemodynamic point of view, it could be tortuosity of the aorta, or inherent differences of flow patterns between the supra- and infra-renal aorta.[10] Indeed, we have observed retrograde flow from the iliac arteries in late systole. We presume this retrograde flow from the iliac arteries more evidently occurs in arteriosclerotic individuals due to the decreased arterial compliance of the lower limb. The antegrade aortic flow and retrograde iliac flow collide above the bifurcation of the aorta, and creates chaotic non-laminar flow dynamics above the bifurcation of the aorta.[63]

Concerning the other geometrical factors, i.e., the immediate upper bent angle did not affect WSS or OSI so much as aortic caliber did. It may be because our populations consisted of a relatively smaller upper bent angle with a median value of 25°. However, its local effects do exist in some individual cases (Fig. 6a–6c). The effect of upper bent angle on the WSS or OSI should be disclosed, assessing a larger sample size shortly.

There is an intriguing report that suggests the possibility of decreasing the risk of rupture of AAA through physical exercise.[30] Exercise has been reported to improve the integrity of the WSS in the AAA through increased flow in the lower limbs as well as higher flow velocities in the aorta.[64] The report may reflect the potential use of WSS and OSI as parameters to monitor and prevent atherosclerosis.

One of the limitations of our study is the small sample size. In the design, we adopted contrast enhancement for better boundary definitions with 3D MRA for morphometry as well as for increasing SNR for 4D-flow MRI; however, two patients declined the administration of the contrast media for fear of adverse reactions. A second potential limitation is a limited cardiac phase resolution. Twelve phases/cardiac cycle or around 83 ms/phase was the limitation of 4D-flow MRI in 2008. However, so far as we have dealt with the blood flow velocities in the abdominal aorta (such as 15 mm/phase for undilated aorta or 5.9 mm/phase for dilated aorta), its streamline delineations are quite similar to the results of CFD simulations using very high spatial and temporal resolutions. The third limitation is the limited spatial resolution. Even if we had used 3D Fourier transform reconstruction algorithm, the partition thickness that reflected the spatial resolution in the Z-axis was limited to 2 mm, which was to cover the entire abdominal aorta within a reasonable scan time. WSS may be underestimated due to the limited spatial resolution. The last potential limitation is that the boundary of the aortic wall was determined by contrast-enhanced MRA, which reflects the averaged signal throughout the cardiac cycle may not be able to reflect compliant aortic wall perfectly. However, the median age of our patient population was around 70 years, and they were all affected by pre-existing arteriosclerosis. Therefore, in all cases, the compliance of the aortic wall was significantly limited compared with non-atherosclerotic younger subjects who are free of vascular disease. According to Astrand et al.,[65] assessment of the healthy non-smoker subjects age over 67 revealed the mean difference of aortic diameter between diastole and systole is 0.67 mm in healthy men and 0.65 mm in healthy women. Similarly, concerning the patients with AAA, the average distensability is 0.9–1.7 mm for the aneurysm.[66–68] We also assessed the movement of the aortic wall by magnitude images for cardiac phases, which were 2.9% of the diameter was within the limit of our spatial resolution (2 mm) for 4D-flow MRI. We, therefore, assume the error due to

the pulsatile movements in this study is not critical, but within the acceptable range.

Conclusion

There are non-laminar flow (i.e., vortex or helical flow) and resultant lower WSS and higher OSI in the dilated aorta compared with the undilated upstream abdominal aorta. In this respect, the wall of the dilated aorta is considered to be at further risk of atherogenic drives, and thereby, under the continuous threat of aneurysmal growth. The delineation of disturbed flow patterns and low WSS and high OSI measured more accurately than before by *in vivo* 4D-flow MRI post-processed with flow analysis software may provide a clue to better understanding of the preference of AAA development in the infrarenal abdominal aorta.

Conflicts of Interest

The corresponding author Yasuo Takehara is an endowed chair of Nagoya University supported by a private company; however, the status is irrelevant to the contents of the paper. Coauthors Tetsuya Wakayama and Atsushi Nozaki are employees of GE Healthcare. The other coauthors have nothing to disclose related to the current study.

References

1. Go AS, Mozaffarian D, Roger VL, et al. Heart disease and stroke statistics—2014 update: a report from the American Heart Association. Circulation 2014; 129:e28–e292.
2. Golledge J, Norman PE. Atherosclerosis and abdominal aortic aneurysm: cause, response, or common risk factors? Arterioscler Thromb Vasc Biol 2010; 30:1075–1077.
3. Porat RM, Grunewald M, Globerman A, et al. Specific induction of tie1 promoter by disturbed flow in atherosclerosis-prone vascular niches and flow-obstructing pathologies. Circ Res 2004; 94:394–401.
4. Fleming C, Whitlock EP, Beil TL, Lederle FA. Screening for abdominal aortic aneurysm: a best-evidence systematic review for the U.S. Preventive Services Task Force. Ann Intern Med 2005; 142:203–211.
5. Clouse WD, Hallett JW, Schaff HV, Gayari MM, Ilstrup DM, Melton LJ. Improved prognosis of thoracic aortic aneurysms: a population-based study. JAMA 1998; 280:1926–1929.
6. Brewster DC, Cronenwett JL, Hallett JW, et al. Guidelines for the treatment of abdominal aortic aneurysms. Report of a subcommittee of the Joint Council of the American Association for Vascular Surgery and Society for Vascular Surgery. J Vasc Surg 2003; 37:1106–1117.
7. Friedman MH, Hutchins GM, Bargeron CB, Deters OJ, Mark FF. Correlation between intimal thickness and fluid shear in human arteries. Atherosclerosis 1981; 39:425–436.
8. Ku DN, Giddens DP, Zarins CK, Glagov S. Pulsatile flow and atherosclerosis in the human carotid bifurcation.

Positive correlation between plaque location and low oscillating shear stress. Arteriosclerosis 1985; 5:293–302.

9. Malek AM, Alper SL, Izumo S. Hemodynamic shear stress and its role in atherosclerosis. JAMA 1999; 282:2035–2042.

10. Moore JE, Maier SE, Ku DN, Boesiger P. Hemodynamics in the abdominal aorta: a comparison of *in vitro* and *in vivo* measurements. J Appl Physiol 1994; 76:1520–1527.

11. Moore JE, Ku DN. Pulsatile velocity measurements in a model of the human abdominal aorta under resting conditions. J Biomech Eng 1994; 116:337–346.

12. Pedersen EM, Agerbaek M, Kristensen IB, Yoganathan AP. Wall shear stress and early atherosclerotic lesions in the abdominal aorta in young adults. Eur J Vasc Endovasc Surg. 1997; 13:443–451.

13. Sho E, Sho M, Hoshina K, Kimura H, Nakahashi TK, Dalman RL. Hemodynamic forces regulate mural macrophage infiltration in experimental aortic aneurysms. Exp Mol Pathol 2004; 76:108–116.

14. Ando J, Yamamoto K. Vascular mechanobiology: endothelial cell responses to fluid shear stress. Circ J 2009; 73:1983–1992.

15. Malek A, Izumo S. Physiological fluid shear stress causes downregulation of endothelin-1 mRNA in bovine aortic endothelium. Am J Physiol 1992; 263:C389–C396.

16. Malek AM, Gibbons GH, Dzau VJ, Izumo S. Fluid shear stress differentially modulates expression of genes encoding basic fibroblast growth factor and platelet-derived growth factor B chain in vascular endothelium. J Clin Invest 1993; 92:2013–2021.

17. Malek AM, Greene AL, Izumo S. Regulation of endothelin 1 gene by fluid shear stress is transcriptionally mediated and independent of protein kinase C and cAMP. Proc Natl Acad Sci USA 1993; 90:5999–6003.

18. Malek AM, Izumo S. Molecular aspects of signal transduction of shear stress in the endothelial cell. J Hypertens 1994; 12:989–999.

19. Malek AM, Izumo S. Control of endothelial cell gene expression by flow. J Biomech 1995; 28:1515–1528.

20. Malek AM, Izumo S. Mechanism of endothelial cell shape change and cytoskeletal remodeling in response to fluid shear stress. J Cell Sci 1996; 109:713–726.

21. Malek AM, Jackman R, Rosenberg RD, Izumo S. Endothelial expression of thrombomodulin is reversibly regulated by fluid shear stress. Circ Res 1994; 74:852–860.

22. Ando J. [Blood flow modulates vascular endothelial gene expressions]. Tanpakushitsu Kakusan Koso 1996; 41:26–33.

23. Ando J, Kamiya A. Blood flow and vascular endothelial cell function. Front Med Biol Eng 1993; 5:245–264.

24. Ando J, Kamiya A. Flow-dependent regulation of gene expression in vascular endothelial cells. Jpn Heart J 1996; 37:19–32.

25. Ando J, Ohtsuka A, Korenaga R, Kawamura T, Kamiya A. Wall shear stress rather than shear rate regulates cytoplasmic Ca++ responses to flow in vascular endothelial cells. Biochem Biophys Res Commun 1993; 190:716–723.

26. Ando K, Mitsuiki S, Itoh K, Kusaba H, Soh T, Tsukise A. Development of vasoactive intestinal polypeptide-immunoreactive nerves in the major cerebral arteries of the quail anterior circulation. J Vet Med Sci 2009; 71:1643–1647.

27. Cunningham KS, Gotlieb AI. The role of shear stress in the pathogenesis of atherosclerosis. Lab Invest 2005; 85:9–23.

28. Hwang J, Ing MH, Salazar A, et al. Pulsatile versus oscillatory shear stress regulates NADPH oxidase subunit expression: implication for native LDL oxidation. Circ Res 2003; 93:1225–1232.

29. Sorescu GP, Song H, Tressel SL, et al. Bone morphogenic protein 4 produced in endothelial cells by oscillatory shear stress induces monocyte adhesion by stimulating reactive oxygen species production from a nox1-based NADPH oxidase. Circ Res 2004; 95:773–779.

30. Suh GY, Les AS, Tenforde AS, et al. Hemodynamic changes quantified in abdominal aortic aneurysms with increasing exercise intensity using MR exercise imaging and image-based computational fluid dynamics. Ann Biomed Eng 2011; 39:2186–2202.

31. Markl M, Chan FP, Alley MT, et al. Time-resolved three-dimensional phase-contrast MRI. J Magn Reson Imaging 2003; 17:499–506.

32. Sekine T, Amano Y, Takagi R, Matsumura Y, Murai Y, Kumita S. Feasibility of 4D flow MR imaging of the brain with either Cartesian y-z radial sampling or k-t SENSE: comparison with 4D Flow MR imaging using SENSE. Magn Reson Med Sci 2014; 13:15–24.

33. Sekine T, Takagi R, Amano Y, et al. 4D Flow MR imaging of ophthalmic artery flow in patients with internal carotid artery stenosis. Magn Reson Med Sci 2018; 17:13–20.

34. Watanabe T, Isoda H, Fukuyama A, et al. Accuracy of the flow velocity and three-directional velocity profile measured with three-dimensional cine phase-contrast MR imaging: verification on scanners from different manufacturers. Magn Reson Med Sci 2019; 18:265–271.

35. Mano Y, Takehara Y, Sakaguchi T, et al. Hemodynamic assessment of celiaco-mesenteric anastomosis in patients with pancreaticoduodenal artery aneurysm concomitant with celiac artery occlusion using flow-sensitive four-dimensional magnetic resonance imaging. Eur J Vasc Endovasc Surg 2013; 46:321–328.

36. Terada M, Takehara Y, Isoda H, Uto T, Matsunaga M, Alley M. Low WSS and high OSI measured by 3D cine PC MRI reflect high pulmonary artery pressures in suspected secondary pulmonary arterial hypertension. Magn Reson Med Sci 2016; 15:193–202.

37. Takehara Y. 4D-flow when and how? La Radiol Med 2020; accepted for publication (in press).

38. Johnston KW, Rutherford RB, Tilson MD, Shah DM, Hollier L, Stanley JC. Suggested standards for reporting on arterial aneurysms. Subcommittee on Reporting Standards for Arterial Aneurysms, Ad Hoc Committee on Reporting Standards, Society for Vascular Surgery and North American Chapter, International Society for Cardiovascular Surgery. J Vasc Surg 1991; 13:452–458.

39. Griswold MA, Jakob PM, Nittka M, Goldfarb JW, Haase A. Partially parallel imaging with localized sensitivities (PILS). Magn Reson Med 2000; 44:602–609.

40. Liu Z, Moorhead RJ, Groner J. An advanced evenly-spaced streamline placement algorithm. IEEE Trans Vis Comput Graph 2006; 12:965–972.

41. Cheng CP, Parker D, Taylor CA. Quantification of wall shear stress in large blood vessels using Lagrangian interpolation

functions with cine phase-contrast magnetic resonance imaging. Ann Biomed Eng 2002; 30:1020–1032.

42. Masaryk T, Drayer BP, Anderson RE, et al. Cerebrovascular disease. American College of Radiology. ACR Appropriateness Criteria. Radiology 2000; 215:415–435.

43. Isoda H, Ohkura Y, Kosugi T, et al. Comparison of hemodynamics of intracranial aneurysms between MR fluid dynamics using 3D cine phase-contrast MRI and MR-based computational fluid dynamics. Neuroradiology 2010; 52:913–920.

44. He X, Ku DN. Pulsatile flow in the human left coronary artery bifurcation: average conditions. J Biomech Eng 1996; 118:74–82.

45. Glagov S, Rowley DA, Kohut RI. Atherosclerosis of human aorta and its coronary and renal arteries. A consideration of some hemodynamic factors which may be related to the marked differences in atherosclerotic involvement of the coronary and renal arteries. Arch Pathol 1961; 72: 558–571.

46. Passerini AG, Polacek DC, Shi C, et al. Coexisting proinflammatory and antioxidative endothelial transcription profiles in a disturbed flow region of the adult porcine aorta. Proc Natl Acad Sci USA 2004; 101:2482–2487.

47. Robicsek F. Francis Robicsek, MD, PhD: a conversation with the editor. Interview by William Clifford Roberts, MD. Am J Cardiol 2000; 85:1340–1356.

48. Boussel L, Rayz V, McCulloch C, et al. Aneurysm growth occurs at region of low wall shear stress: patient-specific correlation of hemodynamics and growth in a longitudinal study. Stroke 2008; 39:2997–3002.

49. Jou LD, Lee DH, Morsi H, Mawad ME. Wall shear stress on ruptured and unruptured intracranial aneurysms at the internal carotid artery. AJNR Am J Neuroradiol 2008; 29:1761–1767.

50. Ujiie H, Tamano Y, Sasaki K, Hori T. Is the aspect ratio a reliable index for predicting the rupture of a saccular aneurysm? Neurosurgery 2001; 48:495–502; discussion 502–503.

51. Annambhotla S, Bourgeois S, Wang X, Lin PH, Yao Q, Chen C. Recent advances in molecular mechanisms of abdominal aortic aneurysm formation. World J Surg 2008; 32:976–986.

52. Wassef M, Baxter BT, Chisholm RL, et al. Pathogenesis of abdominal aortic aneurysms: a multidisciplinary research program supported by the National Heart, Lung, and Blood Institute. J Vasc Surg 2001; 34:730–738.

53. Wassef M, Upchurch GR, Kuivaniemi H, Thompson RW, Tilson MD. Challenges and opportunities in abdominal aortic aneurysm research. J Vasc Surg 2007; 45:192–198.

54. Oshinski JN, Ku DN, Mukundan S, Loth F, Pettigrew RI. Determination of wall shear stress in the aorta with the use of MR phase velocity mapping. J Magn Reson Imaging 1995; 5:640–647.

55. Oyre S, Pedersen EM, Ringgaard S, Boesiger P, Paaske WP. *In vivo* wall shear stress measured by magnetic resonance velocity mapping in the normal human abdominal aorta. Eur J Vasc Endovasc Surg 1997; 13:263–271.

56. Vergara C, Le Van D, Quadrio M, Formaggia L, Domanin M. Large eddy simulations of blood dynamics in abdominal aortic aneurysms. Med Eng Phys 2017; 47:38–46.

57. Ziegler M, Welander M, Lantz J, et al. Visualizing and quantifying flow stasis in abdominal aortic aneurysms in men using 4D flow MRI. Magn Reson Imaging 2019; 57:103–110.

58. Naveenagrawal. Losses due to sudden changes in flow path; 2011. http://www.brighthub.com/engineering/civil/articles/57194.aspx (accessed May 19, 2011).

59. Takami T. Pipe flows, In: Ishiwata R, editor. Fluid mechanics. 1st ed. Tokyo: The Japan Society of Mechanical Engineers, 2005.

60. Kundu PK, Cohen IM, editor. Boundary layers and related topics. 4 ed. Amsterdam: Elsevier, 2008.

61. Papadopoulos G, Otugen MV. A modified Borda-Carnot relation for the prediction of maximum recovery pressure in planar sudden expansions flows. J Fluids Eng 1998; 120:400–402.

62. Robicsek F, Sanger PW, Taylor FH, Magistro R, Foti E. Pathogenesis and significance of post-stenotic dilatation in great vessels. Ann Surg 1958; 147:835–844.

63. Sugiyama M, Takehara Y, Alley M, et al. 4D-flow enables depictions and quantitative analysis of the characteristic flow fluctuations in the infrarenal aorta and diastolic suction flow in renal arteries. Proceedings of 25th Annual Meeting of International Society of Magnetic Resonance in Medicine, Honolulu, 2017; 2855.

64. Tang BT, Cheng CP, Draney MT, et al. Abdominal aortic hemodynamics in young healthy adults at rest and during lower limb exercise: quantification using image-based computer modeling. Am J Physiol Heart Circ Physiol 2006; 291:H668–H676.

65. Astrand H, Stalhand J, Karlsson J, Karlsson M, Sonesson B, Länne T. *In vivo* estimation of the contribution of elastin and collagen to the mechanical properties in the human abdominal aorta: effect of age and sex. J Appl Physiol 2011; 110:176–187.

66. Arko FR, Murphy EH, Davis CM, Johnson ED, Smith ST, Zarins CK. Dynamic geometry and wall thickness of the aortic neck of abdominal aortic aneurysms with intravascular ultrasonography. J Vasc Surg 2007; 46: 891–896; discussion 896–897.

67. Long A, Rouet L, Vitry F, Albertini JN, Marcus C, Clement C. Compliance of abdominal aortic aneurysms before and after stenting with tissue doppler imaging: evolution during follow-up and correlation with aneurysm diameter. Ann Vasc Surg 2009; 23:49–59.

68. Ganten MK, Krautter U, von Tengg-Kobligk H, et al. Quantification of aortic distensibility in abdominal aortic aneurysm using ECG-gated multi-detector computed tomography. Eur Radiol 2008; 18:966–973.